1 **Supplementary Information to "Global perturbation of the carbon**

2 **cycle at the onset of the Miocene climatic optimum"**

3

4 Our study is based on lower to middle Miocene marine sediments recovered at

5 IODP Site U1337 (3°50.009′N, 123°12.352′W; 4200 m water depth) in the eastern

6 equatorial Pacific Ocean during the Pacific Equatorial Age Transect (PEAT)

7 Expedition 321 (Supplementary Fig. S1). Detailed site location, core recovery and

8 lithological descriptions are provided in Pälike et al. (2010). This work extends

9 middle Miocene benthic foraminiferal isotope studies in Site U1337 (Tian et al.,

10 2013) and Site U1338 (Holbourn et al., 2014).

11

12 **Sampling strategy**

13 Cores were sampled in 10 cm intervals (~5 kyr time resolution) from a

14 composite sequence (shipboard splice) from Holes U1337A, U1337C and U1137D

15 (334.46 – 440.43 meters composite depth). Samples were oven dried at 40°C, washed

16 over a 63 µm sieve, then oven dried at 40°C on a sheet of filter paper.

17

18 **Astronomically-tuned chronology**

19 Astronomical tuning and calculation of sedimentation rates were performed

20 with AnalySeries 2.0.4.2 (Paillard et al., 1996). We correlated $\delta^{18}O$ minima to

21 ET+0.2P maxima, following a minimal tuning strategy to preserve original spectral

22 characteristics. The benthic isotope data set from Site U1337 is plotted against

23 composite depth and against age in Supplementary Fig. S2. Age tie points between

24 the $\delta^{18}O$ series and the ETP target (Laskar et al., 2004) are shown in Supplementary

25   Fig. S2 and Supplementary Table S1. The average sedimentation rate is ~2 cm kyr^{-1},

26   corresponding to an average chronological resolution of ~5 kyr.

27   Comparison of the δ^{18}O curves plotted against depth and age shows that original

28   spectral characteristics are retained following the tuning procedure. We note that the

29   short eccentricity cycle (100 kyr) is prominently imprinted in the δ^{18}O and δ^{13}C

30   records (Supplementary Figs. S2-S3). Superimposed on higher frequency variations,

31   the 400 kyr eccentricity cycle is additionally encoded in the δ^{13}C record

32   (Supplementary Fig. S3). The detection of the 100 and 400 kyr eccentricity cycles in

33   the δ^{13}C series supports the age model, based on independent tuning of the δ^{18}O

34   series.

35   Comparison of astronomically-calibrated benthic isotope series from Site

36   U1337 and subantarctic Atlantic Ocean Site 1090 (Billups et al., 2002; 2004)

37   indicates that the independent age models are overall compatible (Supplementary Fig.

38   S4). The marked δ^{18}O and δ^{13}C decreases marking the onset of the MCO in Site

39   U1337 are identified in Site 1090, further supporting the global nature of these events.

40   The apparent temporal offset at the onset of the δ^{18}O and δ^{13}C decreases is most likely

41   due to the incompleteness of the Site 1090 over this interval.

42

43   **Benthic foraminiferal and bulk carbonate δ^{18}O and δ^{13}C**

44   Between 17.2 and 15.5 Ma, benthic foraminiferal and bulk carbonate δ^{18}O have

45   means of 1.33 ‰ and -0.25 ‰ with standard deviation of 0.30 ‰, and 0.29 ‰,

46   respectively. Benthic and bulk carbonate δ^{13}C have means of 1.13 ‰ and 1.94 ‰

47   with standard deviation of 0.33 and 0.29 ‰, respectively. The offset in mean values

48   reflects the different origins of the source materials, as the bulk carbonate (lighter

49    $\delta^{18}O$, heavier $\delta^{13}C$) represents a near surface signal, primarily based on calcareous

50   nannofossils derived from surface-dwelling algae. The benthic and bulk carbonate

51    $\delta^{18}O$ and $\delta^{13}C$ records show a marked co-variance in the 100 kyr eccentricity band

52   from 17.2 to 15.5 Ma (Fig. 2, Supplementary Figs. S2-S3). This is particularly

53   striking for the prominent $\delta^{18}O$ minima at 16 and 15.6 Ma, which coincide with sharp

54    $\delta^{13}C$ minima.

55   We checked the abundance, distribution and preservation of calcareous

56   nannofossils in selected samples with different carbonate contents, using a scanning

57   electron microscope. We found that abundance decreased slightly with carbonate

58   content, but that assemblage composition (size and taxonomic groups) and

59   preservation did not differ markedly. Thus, we concluded that the bulk carbonate

60   isotope signals are not primarily influenced by changes in assemblage composition

61   due to selective dissolution.

62

63   **REFERENCES**

64   Billups, K., Channell, J.E.T., and Zachos, J., 2002, Late Oligocene to early Miocene

65   geochronology and paleoceanography from the sub-Antarctic South Atlantic:

66   Paleoceanography, v. 17, 1004, doi:10.1029/2000PA000568.

67   Billups, K., Pälike, H., Channell, J.E.T., Zachos, J.C., and Shackleton, N.J., 2004,

68   Astronomic calibration of the late Oligocene through early Miocene geomagnetic

69   polarity time scale: Earth and Planetary Science Letters, v. 224, p. 33-44,

70   doi:10.1016/j.epsl.2004.05.004.

71   Holbourn, A.E., Kuhnt, W., Lyle, M.W., Schneider, L., Romero, O., and Andersen.

72   N., 2014, Middle Miocene climate cooling linked to intensification of eastern

73   equatorial Pacific upwelling: Geology, v. 42, p. 19-22, doi:10.1130/G34890.1.

74 Laskar, J., Robutel, P., Joutel, F., Gastineau, M., Correia, A., and Levrard, B., 2004,

75   A long-term numerical solution for the insolation quantities of the Earth:

76   Astronomy and Astrophysics, v. 428, p. 261-285, doi:10.1051/0004-

77   6361:20041335.

78 Paillard, D., Labeyrie, L., and Yiou, P., 1996, Macintosh program performs time-

79   series analysis: EOS Transactions AGU, v. 77, p. 379.

80 Pälike, H., Lyle, M.W., Nishi, H., Raffi, I., Gamage, K., Klaus, A., and the Expedition

81   320/321 Scientists, 2010, Proceedings of the Integrated Ocean Drilling Program,

82   320/321: Tokyo, Integrated Ocean Drilling Program Management International,

83   Inc., doi:10.2204/iodp.proc.320321.109.2010.

84 Tian, J., Yang, M., Lyle, M.W., Wilkens, R., and Schackford, J.K., 2013, Obliquity

85   and long eccentricity pacing of the Middle Miocene climate transition:

86   Geochemistry, Geophysics, Geosystems, v. 14, p. 1740-1755,

87   doi:10.1002/ggge.20108.

88 Woodruff, F., and Savin, S., 1991, Mid-Miocene isotope stratigraphy in the deep sea:

89   high resolution correlations, paleoclimatic cycles, and sediment preservation:

90   Paleoceanography, v. 6, p. 755-806.

91

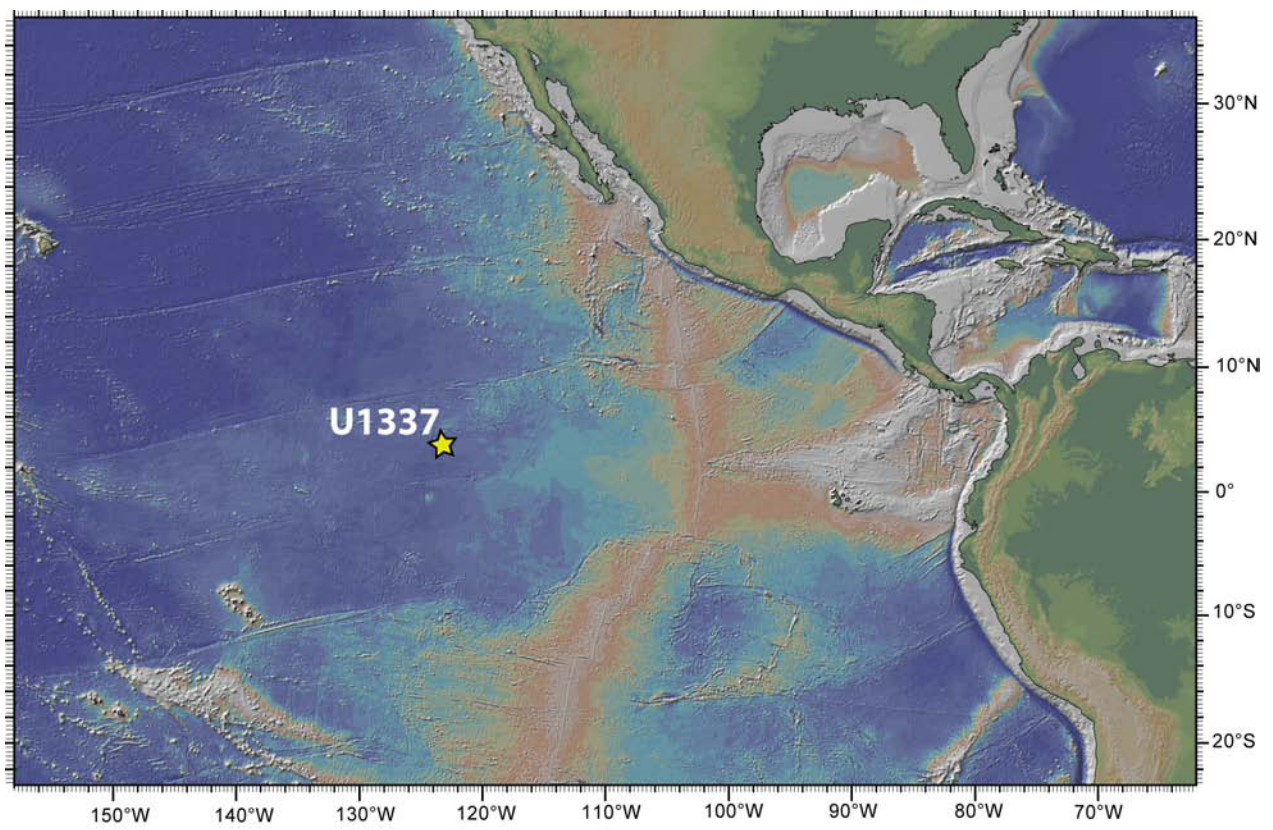92 **CAPTIONS FOR SUPPLEMENTARY FIGURES AND TABLE**

93

94 **Supplementary Figure 1.** Map showing the present day location of IODP Site U1337

95 in the eastern equatorial Pacific (3°50.009′N, 123°12.352′W; 4200 m water depth).

96 Site U1337 was located SW of its present position, within ±2° of the Equator between

97 8 and 24 Ma (Pälike et al., 2010).

98

99   **Supplementary Figure 2.** (a) U1337 benthic δ^{18}O versus meters composite depth

100   (mcd). (b) Comparison of 400 kyr filtered eccentricity (centered at frequency 0.0025

101   with bandwidth 0.0005) and benthic δ^{13}C. (c) Sedimentation rates. (d) U1337 benthic

102   δ^{18}O versus age. (e) Eccentricity-tilt-precession (ETP) tuning target from Laskar et al.

103   (2004). Tie points are indicated by black crosses.
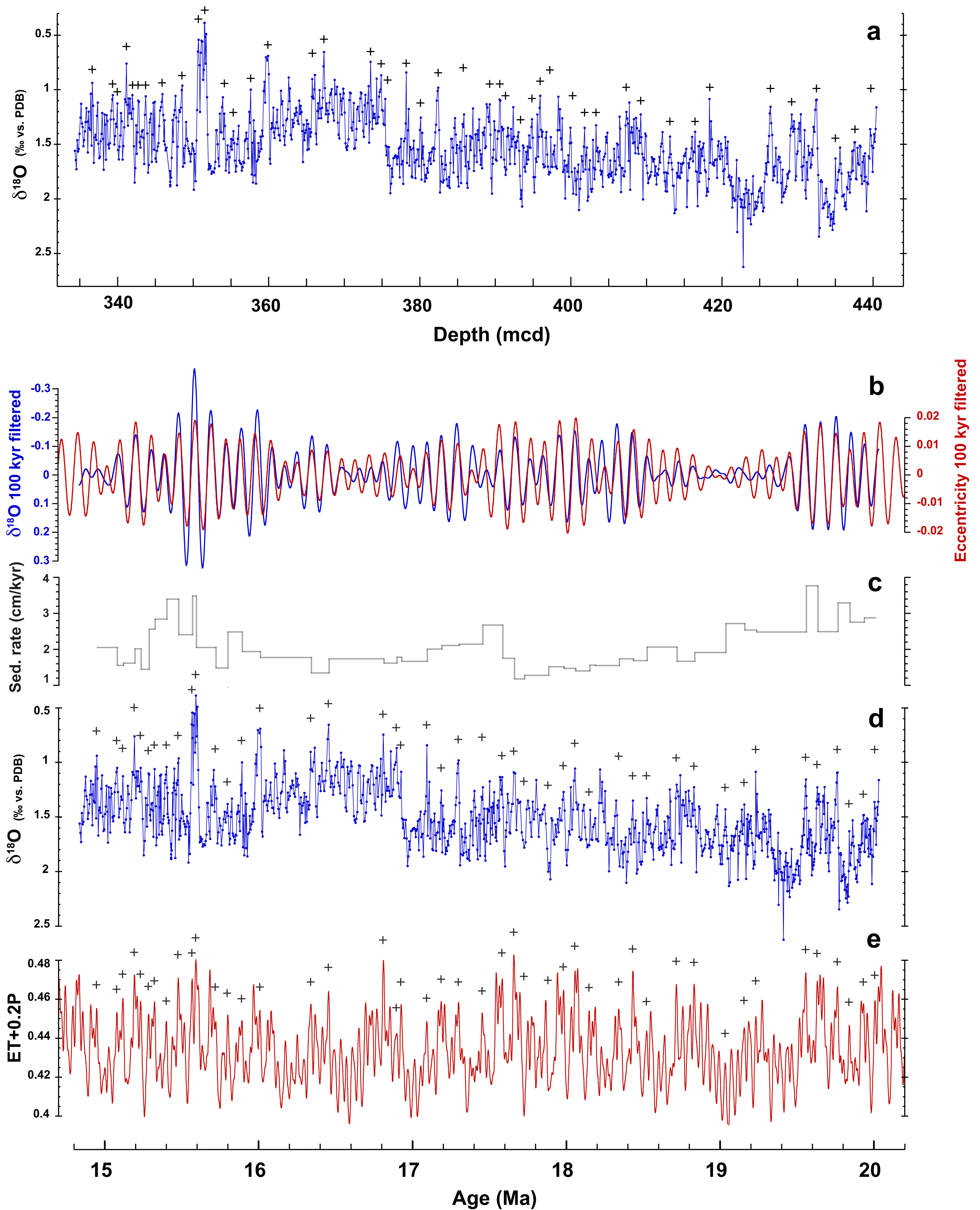
104

105   **Supplementary Figure 3.** (a) Comparison of 400 kyr filtered eccentricity (centered at

106   frequency 0.0025 with bandwidth 0.0005) and benthic δ^{13}C. (b) Comparison of 100

107   kyr filtered eccentricity (centered at frequency 0.01 with bandwidth 0.004) and

108   benthic δ^{13}C from IODP Site U1337. (c) Benthic δ^{13}C from IODP Site U1337.

109

110   **Supplementary Figure 4.** Comparison of U1337 benthic δ^{18}O and δ^{13}C with

111   independently age calibrated records from ODP Site 1090, subantarctic Atlantic

112   Ocean (Billups et al., 2002; 2004). (a) Benthic δ^{13}C from ODP Site 1090. (b) Benthic

113   δ^{13}C from IODP Site U1337. (c) Benthic δ^{18}O from ODP Site 1090. (d) Benthic δ^{18}O

114   from IODP Site U1337. PDB: PeeDee Belemnite, MCO: Miocene Climatic Optimum.

115   Purple crosses mark prominent correlative features. Lilac shading marks sharp δ^{18}O

116   decreases coincident with negative shift in δ^{13}C (shaded orange).
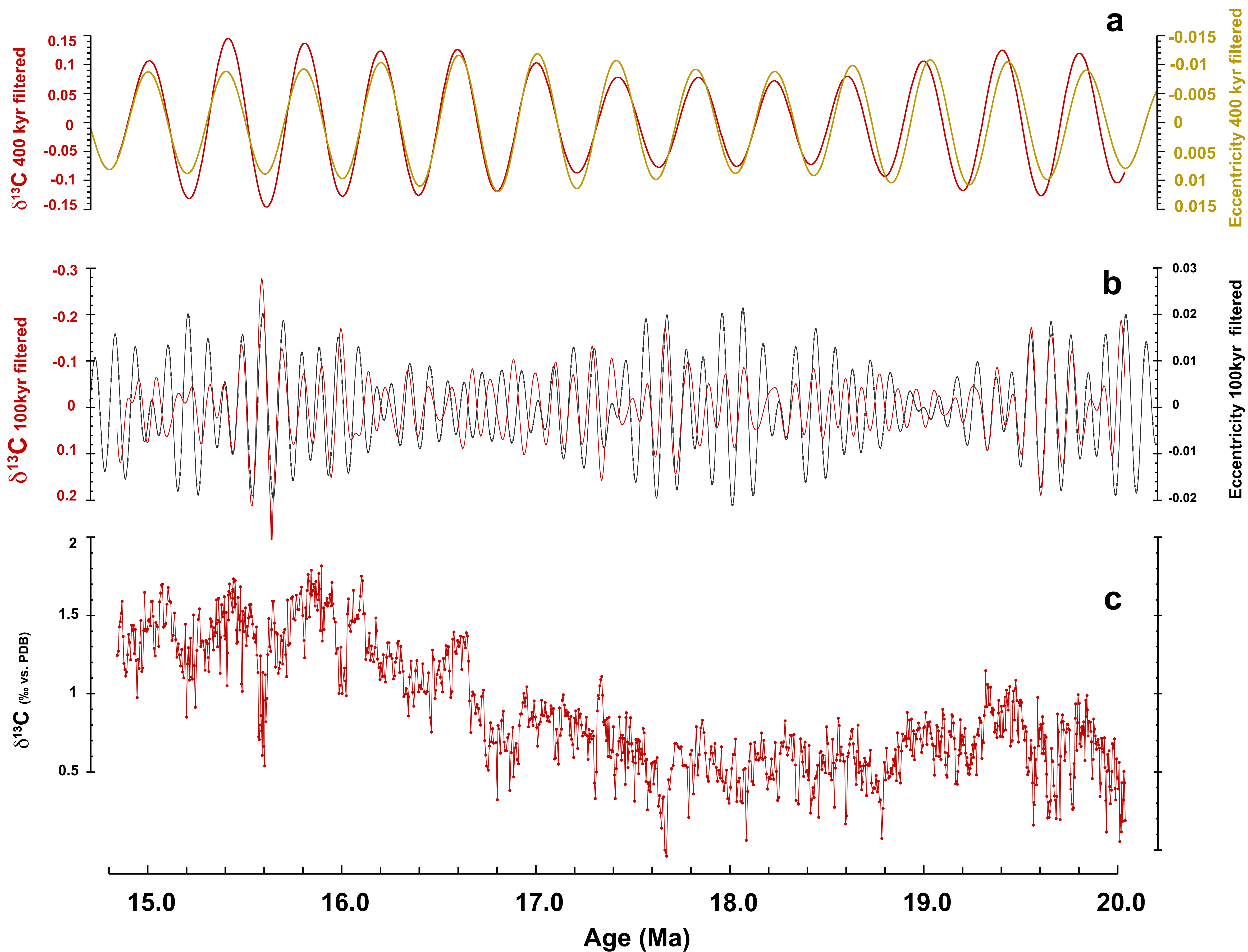
117

118   **Supplementary Table 1.** Age control points used to derive astronomically tuned

119   timescale in IODP Site U1337.

Supplementary Figure S1

Supplementary Figure S2

Supplementary Figure S3

a δ¹³C (‰ vs. PDB) — 1090

b δ¹³C (‰ vs. PDB) — U1337 — onset of "Monterey Excursion"

c δ¹⁸O (‰ vs. PDB) — 1090

d δ¹⁸O (‰ vs. PDB) — U1337 — onset of MCO

Age (Ma)
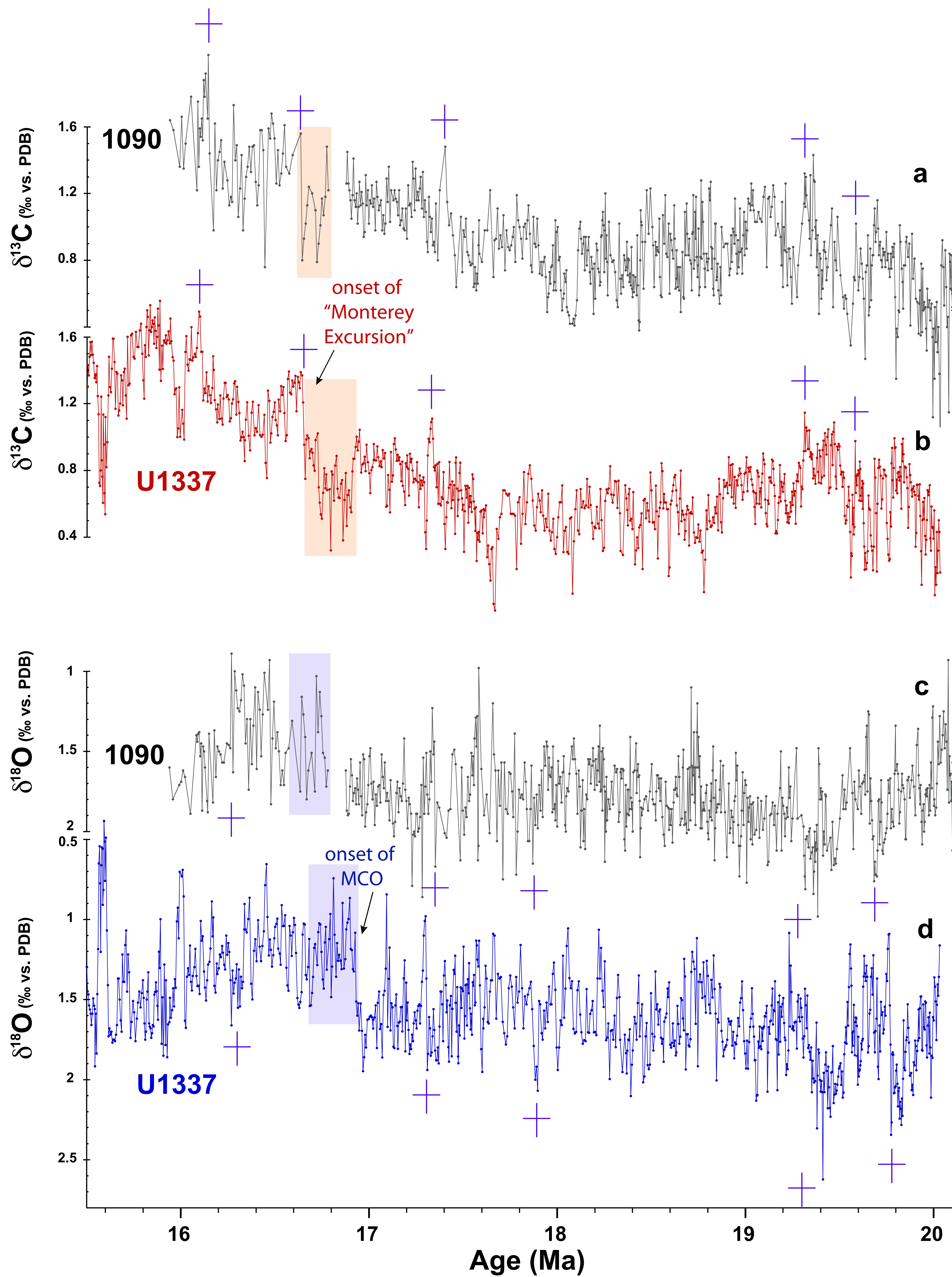
Supplementary Figure S4

Supplementary Table 1

Depth (mcd)	Age (ka)
336.66	14949
339.35	15080
339.96	15119
341.17	15194
341.97	15234
342.72	15286
343.72	15325
345.91	15402
348.52	15479
350.69	15569
351.55	15594
354.15	15721
355.31	15799
357.62	15892
359.9	16010
365.79	16341
367.33	16456
373.5	16812
374.89	16898
375.41	16927
378.21	17095
380.11	17189
382.46	17301
385.76	17455
389.25	17585
390.58	17661
391.35	17727
393.36	17884
394.85	17983
395.95	18058
397.24	18150
400.24	18343
401.82	18434
403.32	18523
407.32	18717
409.25	18832
413.11	19035
416.46	19158
418.39	19234
426.42	19558
429.24	19632
432.51	19764
435.04	19841
437.61	19934
439.73	20008